Applied Materials Today 5 (2016) 142–149

Contents lists available at ScienceDirect

Applied Materials Today

journal homepage: www.elsevier.com/locate/apmt

Organic adsorbates have higher affinities to fluorographene than to graphene

Eva Otyepková, Petr Lazar, Klára Čépe, Ondřej Tomanec, Michal Otyepka*

Regional Centre of Advanced Technologies and Materials, Department of Physical Chemistry, Faculty of Science, Palacký University Olomouc, tř. 17. Listopadu 12, 771 46 Olomouc, Czech Republic

ARTICLE INFO

Article history:
Received 1 September 2016
Received in revised form
24 September 2016
Accepted 24 September 2016

Keywords:
Enthalpy
Entropy
IGC
Graphene
Fluorographene

ABSTRACT

The large surfaces of two-dimensional carbon-based materials, such as graphene and fluorographene, are exposed to analytes, impurities and other guest molecules, so an understanding of the strength and nature of the molecule–surface interaction is essential for their practical applications. Using inverse gas chromatography, we determined the isosteric adsorption enthalpies and entropies of six volatile organic molecules (benzene, toluene, cyclohexane, *n*-hexane, 1,4-dioxane, and nitromethane) to graphene and graphite fluoride powders. The adsorption entropies of the molecules ranged from −17 to −34 cal/mol K and the maximum adsorption-induced entropy loss occurred for nitromethane at the high-energy sites. The enthalpies of bulkier adsorbates were almost coverage-independent on both surfaces and ranged from −11 to −14 kcal/mol. Despite the fact that fluorographene has lower surface energy than graphene and graphene represents an ideal surface for the π–π stacking, the adsorbates had lower adsorption enthalpies to fluorographene than to graphene by ~9%. These findings imply that bulkier airbone organic contaminants readily adsorb to the investigated surfaces and can modify the measured surface properties.

1. Introduction

Graphene's capacity to adsorb small molecules [1] is one of its most important properties and is widely exploited in its practical applications [2,3]. Because small molecule adsorption changes the electronic properties of graphene [4], devices based on graphene-type materials could be sensitive sensors of guest molecules [5–7]. The adsorption of organic molecules affects also the surface properties of graphene [8] such as its hydrophobicity [9,10], which would in turn affect its use and performance in all field, where the surface of graphene is involved, e.g., coating-technologies, electrochemistry, catalysis, and lubrication. Graphene is also regarded as a useful adsorbent in applications such as pollutant removal and drug delivery [11–14]. Noncovalent interactions to graphene also affect its colloidal stability, dispersability and processability of graphene dispersions [15,16]. The mentioned applications fueled research of graphene's surface properties and affinity of guest molecules to graphene.

In 2010, fluorographene was synthesized via the fluorination of graphene and mechanical and chemical exfoliation of graphite fluoride [17–19]. It was initially considered to be a rather inert material, analogous to Teflon. However, recent experiments have revealed that it is reactive under ambient conditions and, consequently, can be utilized as a starting material for the preparation of graphene derivatives [20–23]. The surface properties of fluorographene have not been explored so extensively as those of graphene, although various interesting features have been observed. Graphite fluoride has a lower surface energy than graphite [24], and has been used as an industrial lubricant for over forty years [25]. However, fluorination of graphene yields materials exhibiting nontrivial friction behavior [26]. Graphite fluoride, fluorographene, and partially fluorinated graphenes have been successfully used as electrochemical detectors [27–32] whose performance is driven by their conductivities and the analyte's adsorption to the electrode surface [28]. For a broad application of fluorinated graphenes in practice, it is necessary to take into account a potential hazard for human cells. Pioneering studies on cell lines identified some risks associated with interaction of fluorinated graphenes with cells, which was dependent on size and degree of fluorination [33,34], on the other hand, the toxicity of the respective materials is still significantly underexplored.

Both graphene and fluorographene are 2D hydrophobic materials. In their 3D analogues, i.e., graphite and graphite fluoride, the layers are bound by the London dispersive forces [24,35]. Both surfaces, however, differ, as graphene is flat surface of a honeycomb lattice of the sp^2 carbon atoms with π-electron clouds above and below the carbon layer [36], ideally suited for π–π stacking interactions [37,38]. On the other hand, fluorographene has the hexagonal lattice made of the sp^3 carbon atoms, to which the fluorine atoms are attached. In addition, the covalent C–F bond is rather polar [39]

* Corresponding author.
E-mail address: michal.otyepka@upol.cz (M. Otyepka).

http://dx.doi.org/10.1016/j.apmt.2016.09.016

imprinting some electrostatic filed across the fluorographene plane [40]. The question is how the distinct properties of graphene and fluorographene influence their adsorption behavior.

In this paper, we study the adsorption properties of graphene and fluorographene using inverse gas chromatography (IGC). IGC measures the retention of probe molecules (adsorbates) in a column loaded with the adsorbent, and the surface-energy and adsorption enthalpy and entropy can be determined from the resulting retention curves [41–46]. IGC is dominantly used for measurement of the surface energy and its ability to determine the adsorption enthalpy and entropy is often being overlooked. IGC has couple of advantages over other experimental techniques, e.g., it provides an averaged response of the material, and enables to manipulate with the targeted coverage of the adsorbent. The targeted coverage of the adsorbent allows determining the dependence of the isosteric adsorption enthalpy on the coverage, and to study microscopic processes related to the adsorption, identify the high-energy sites, etc.

Using the IGC technique, we compared the adsorption of six volatile organic molecules to graphene and graphite fluoride powders. For the measurements, we used nitromethane as a small molecular probe and five similarly sized organic molecules, one aliphatic (*n*-hexane), two alicyclic (cyclohexane and 1,4-dioxane), and two aromatic (benzene and toluene). Applying the Langmuir adsorption model we determined the corresponding isosteric adsorption enthalpies and entropies as a function of the surface coverage (ranging from 0.5% to 18% of a monolayer). We used IGC to determine both the isosteric adsorption enthalpies and entropies. The experimental findings were interpreted with the help of density functional theory (DFT) calculations, which may provide useful insights into strength and nature of interaction to 2D materials [8,47].

2. Experimental

2.1. Materials

We used a graphene powder (A01, GrapheneSupermarket) that has been extensively characterized using various experimental techniques in our previous studies [8,48]. It consists of 3-nm (height) graphene flakes with a high surface area (915 m^2/g) [48] and a diameter of only a few micrometers. The graphite fluoride powder (Sigma–Aldrich) had a surface area of 236.9 m^2/g (see [24]) and consisted of flaky lamellar crystals, with a terrace height of 10–15 nm. We used volatile organic molecules as adsorbents; these included: *n*-hexane (Merck, LiChrosolv for LC, ≥98%), toluene (Sigma–Aldrich, Chromasolv for HPLC, 99.9%), 1,4-dioxane (Sigma–Aldrich, Chromasolv Plus for HPLC, ≥99.5%), benzene (Sigma–Aldrich, Chromasolv for HPLC, ≥96%), cyclohexane (Sigma–Aldrich, Chromasolv Plus for HPLC, ≥99.9%), and nitromethane (Sigma–Aldrich, Chromasolv for HPLC, 99.9%).

2.2. Microscopic measurements

Samples were characterized via transmission electron microscopy (TEM; JEOL 2100 equipped with a LaB6 electron gun), at an accelerating voltage of 200 kV. The corresponding images were obtained by using a Tengra (EMSIS) camera. Samples for TEM analyses were prepared by dispersing graphite fluoride/graphene nanopowder in ethanol and sonicating for 5 min. One drop of the resulting solution was placed on a copper grid, covered with a holey carbon film, and dried at room temperature. Scanning electron microscope (SEM; SEM Hitachi SU6600 equipped with a Schottky electron source) images of the dried drop were obtained at an accelerating voltage of 5 kV, in secondary electron (SE) mode. Samples for SEM analyses were affixed to conductive carbon tape and placed in an aluminum holder. The surface topologies of these samples were evaluated via scanning probe microscopy (SPM) in semi-contact atomic force microscopy (AFM; Ntegra, NT-MDT) mode, using an Ha_NC probe. Similarly, high-resolution TEM (HR-TEM, Titan, FEI) elemental maps of the samples were obtained in scanning transmission electron microscopy (STEM) mode (80 keV) using a Super-X energy-dispersive detector (EDS; Bruker).

2.3. IGC setup and data fitting

IGC experiments were performed using a surface energy analysis instrument (SEA; SMS-iGC 2000 equipped with Cirrus – SEA Control Software, Version 1.3.3.2, Surface Measurement Systems Ltd., UK 2011); the resulting chromatograms were all processed by CirrusPlus (SEA Data Analysis Software, Version 1.2.1.2, Surface Measurement Systems Ltd., UK, 2012). For the experiments, 18.8 mg of graphene powder or 23.9 mg of graphite fluoride powder were loaded into 30-cm-long silylated glass columns and were washed by helium gas for 2 h (10 sccm helium carrier gas, at 80 °C) prior the experiments. The partial pressures were determined from adsorbate peak maxima, based on instrument calibration, and the temperature of the column was controlled by an instrument oven with a declared stability of ±0.1 °C. The coverage was controlled by the injection time of the adsorbate vapor, which was calculated from the surface area and vapor tension of the adsorbate at 40 °C. The isosteric adsorption enthalpies and entropies were fitted using the following equation [46]:

$$K = \frac{\upsilon}{(1-\upsilon)p/p^0} = e^{-(\Delta H_{ad} - T\Delta S_{ad})/RT)}$$

where K, υ, p, p^0, ΔH_{ad}, ΔS_{ad}, R, and T are the equilibrium constant, coverage, pressure, standard pressure, isosteric (at the given υ) adsorption enthalpy, isosteric adsorption entropy, universal gas constant, and temperature, respectively. The chromatograms were used for fitting only for net retention times (vs. methane) of >0.26 min (i.e., greater than 3σ of the methane peak fitted by a Gaussian distribution).

2.4. DFT calculations

The projector-augmented wave method, as implemented in the Vienna ab-initio simulation package (VASP) suite, was used for the calculations [49,50]. The energy cutoff for the plane-wave expansion was set to 400 eV. Moreover, the interaction energy and forces were calculated by applying the optimized van der Waals functional optB86b-vdW [51], which encompasses both local and non-local electron–electron correlation effects, such as London dispersive forces [8]. The graphene and fluorographene sheets were modeled by a 6×6 supercell (72 carbon atoms, or 72 carbon and 72 fluorine atoms) and the forces between the surface and the molecule were fully relaxed. In addition, the periodically repeated sheets were separated by at least 16 Å of vacuum, and a $3 \times 3 \times 1$ k-point grid was used to sample the Brillouin zone. The thermal corrections for the enthalpy were taken from our previous work [8]. The polarizabilities of molecules were calculated by applying the electric field (LCALCEPS tag in VASP) as the ratio of the change of the dipole moment to the magnitude of electric field (dP/dE).

3. Results and discussion

3.1. Structural features of graphene and fluorographite powders

Both nanomaterials were analyzed by a wide range of microscopic and spectroscopic techniques as part of our previous studies

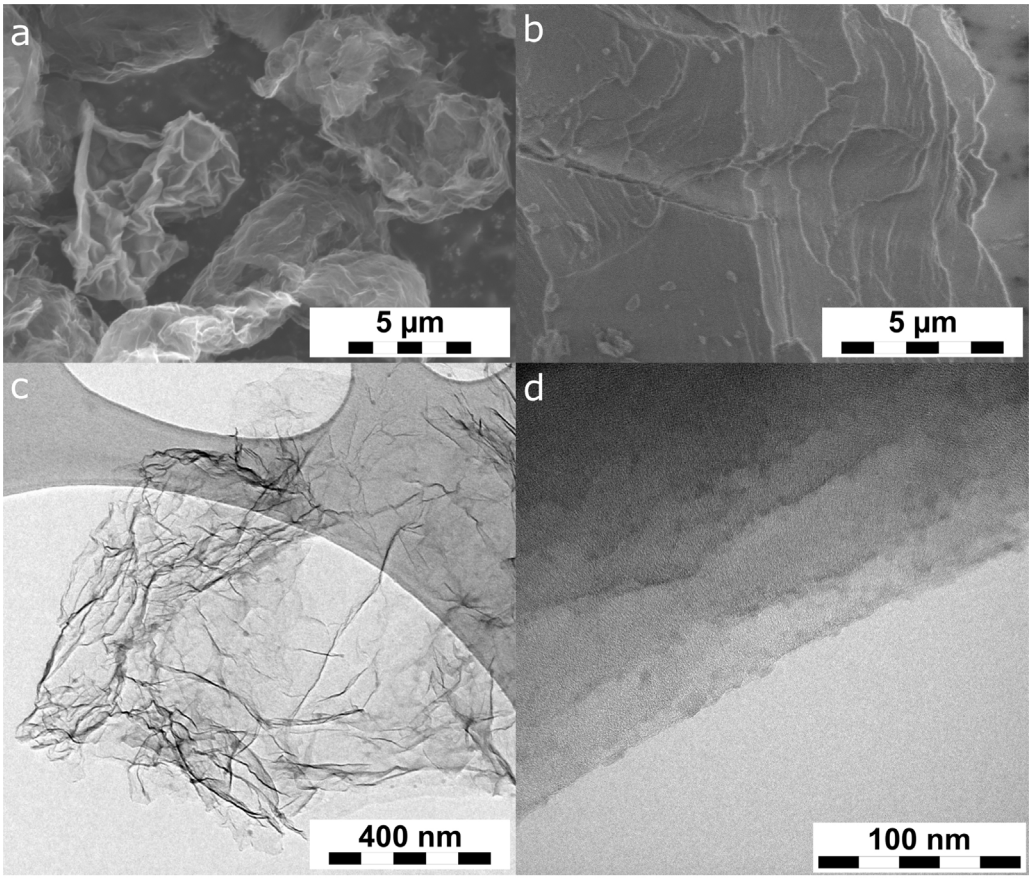

Fig. 1. SEM and TEM images of the (a, c) graphene nanopowder and (b, d) graphite fluoride flakes.

[8,24,46,48]. The graphene nanopowder consists of 3-nm-thick, crumpled flakes (see Fig. 1a and c), with Raman characteristics comparable to those of few-layer graphene and a distinct few-lamellar structure [48]. The graphite fluoride also has a lamellar structure with significantly exposed fluorographene terraces (see Figs. 1b, d, and 2), and the individual lamellae consist of homogeneously distributed carbon and fluorine atoms (Fig. 2). The lateral size of individual graphite fluoride flakes as determined by SEM amounts to ~15 μm × 25 μm (Fig. S1 in Supporting Information) with vertical heights of ~7 μm.

3.2. Adsorption enthalpies of graphene

We measured the isosteric adsorption enthalpies of six volatile organic molecules at coverage values ranging from 0.25% to 20% of monolayer to both graphene and fluorographene. It should be noted that the experimental setup allowed a maximum coverage value of 3% and 7% for nitromethane on graphene and fluorographene, respectively. The adsorption enthalpies of both materials exhibited a weak dependence (see Fig. 3) on the coverage over the entire range of coverages investigated. However, the adsorption enthalpy of nitromethane decreased sharply at coverages ranging from 0.25% to 1.00%. We assume that the decrease occurred due to the adsorption of nitromethane into high-energy adsorption sites in the graphene powder. This result concurs with our previous finding [48] that the investigated graphene powder contained 0.24 ± 0.03% high-energy sites (in that case, steps and cavities [48]), as determined from adsorption experiments with acetone. The enthalpy-coverage profiles for larger molecules did not indicate the presence of any high-energy sites. In order to corroborate this hypothesis, we performed DFT calculation of adsorption of benzene on the step-like defect. The step-like defect was very energetically favorable in the case of acetone and ethanol molecules [46,48]. The DFT calculation unveiled that the binding of benzene to step was only slightly (by 20%) more favorable than the binding to the graphene surface. Such a moderate energetic gain and greater size of the molecule suppress the role of high-energy sites.

The adsorption enthalpies reached a steady state at surface coverage values of >2% (Fig. 3). At this range of coverage, the adsorption enthalpy of graphene and graphite stems from adsorption to the graphene surface [8,46,48]. Therefore, in the current study, we attribute adsorption enthalpies at coverages of >2% to terrace/surface adsorption of both materials. The likelihood of adsorbate–adsorbate interaction increases with increasing coverage, as indicated by the transition of adsorption isotherms from the Langmuir to BET regimes. Hence, we averaged the isosteric adsorption enthalpies measured at 2–10% of monolayer coverage and used these averaged values (see Table 1) thereafter.

The adsorption enthalpy of toluene to graphene was −13.8 ± 0.4 kcal/mol, which is very close to the IGC-determined value of −13.5 ± 0.3 kcal/mol [8] and falls within the range of the TPD-determined enthalpies to highly-oriented pyrolytic graphite (HOPG) (−16.6 ± 1.7 and −13.2 ± 1.4 kcal/mol, for a monolayer (ML) and the fourth ML, respectively, as calculated from the desorption activation energy E_A, $\Delta H_{ad} = -E_A - 1/2RT$ at 323 K) [52]. The measured adsorption enthalpy of benzene to graphene was −11.9 ± 0.3 kcal/mol. Recent thermal-desorption studies of the interaction of polycyclic aromatic hydrocarbon molecules with the basal plane of graphite yield, through the analysis of desorption kinetics, activation energy of 0.50 eV (11.5 kcal/mol) [53] at submonolayer coverages, in excellent agreement with our IGC result.

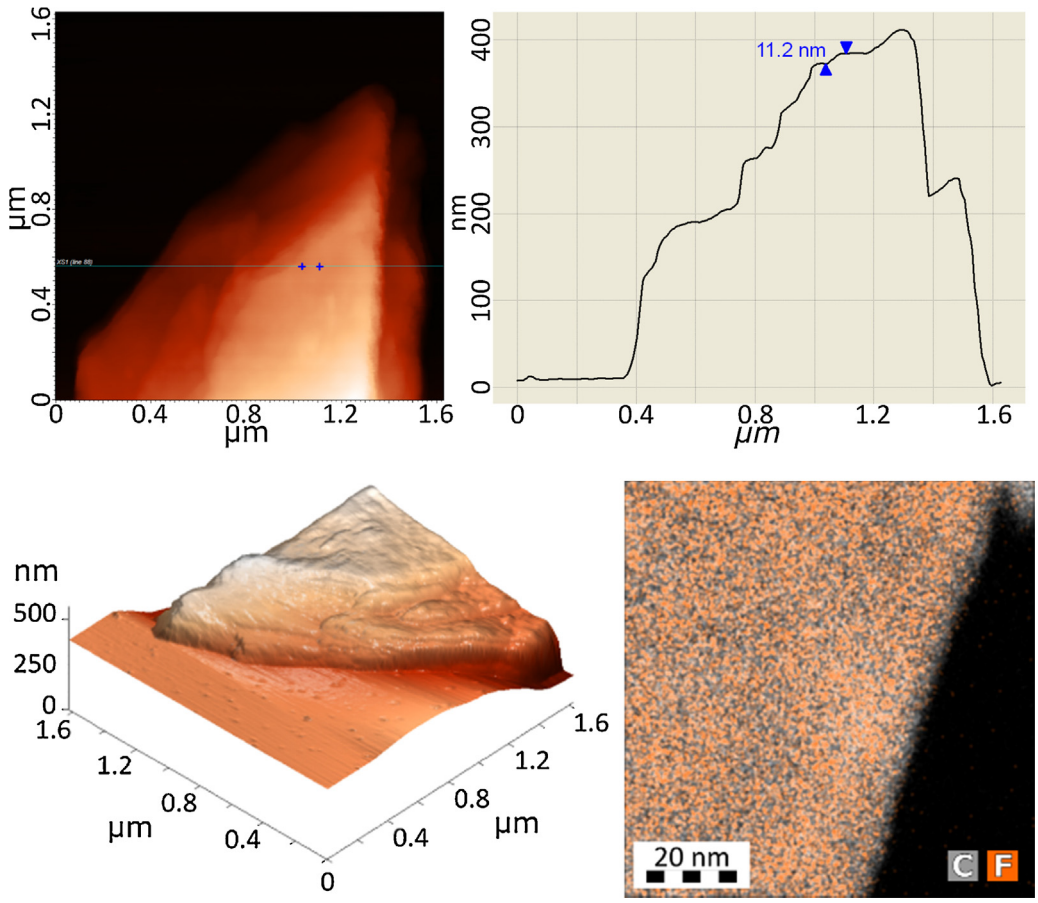

Fig. 2. AFM images and corresponding height profile (upper right panel) reveal the lamellar structure of a graphite fluoride flake with exposed fluorographene terraces. The fluorine atoms are homogeneously distributed over the fluorographene surface, as shown by the elemental map (lower right panel), obtained via HRTEM/EDS.

Table 1
Saturated adsorption enthalpies and entropies to graphene and graphite fluoride powders.

Compound	Graphene		Fluorographene		
	ΔH (kcal/mol)	ΔS (cal/mol K)	ΔH (kcal/mol)	ΔS (cal/mol K)	T_{min}–T_{max} (K)
1,4-Dioxane	−10.8 ± 0.1	−26.9 ± 0.2	−11.7 ± 0.2	−29.9 ± 0.4	313–363
Benzene	−11.9 ± 0.3	−28.0 ± 1.1	−12.7 ± 0.2	−30.1 ± 0.7	313–363
Cyclohexane	−11.4 ± 0.3	−28.0 ± 0.7	−12.2 ± 0.2	−30.4 ± 1.3	313–363
Nitromethane	−6.3 ± 0.1	−16.8 ± 1.1	−9.2 ± 0.2	−25.9 ± 0.8	313–363
n-Hexane	−13.5 ± 0.2	−31.2 ± 0.5	−14.3 ± 0.3	−34.1 ± 0.6	313–363
Toluene	−13.8 ± 0.4	−28.9 ± 1.5	−13.1 ± 0.2	−27.8 ± 0.8	313[a]–363

[a] The temperature interval for graphene powder was 333–363 K.

The lower value obtained for the adsorption enthalpy of *n*-hexane to graphene powder relative to our previously determined [8] value (−13.5 ± 0.2 vs. −12.2 ± 0.2 kcal/mol) can be attributed to the difference in fitting methods; in our previous study [8], we used the linearized Clausius–Clapeyron equation for data fitting. On the other hand, it shows that the error bars assessed from the data fitting could be underestimated and the real experimental uncertainty of the adsorption enthalpies determined by IGC is around 1 kcal/mol. Nonetheless, the close correspondence between the theoretically predicted and measured adsorption enthalpies [8,48] indicate that the IGC technique can reliably determine the adsorption enthalpies of volatile organic compounds to carbonaceous materials.

The higher adsorption enthalpy of cyclohexane, (−11.4 ± 0.3 kcal/mol), compared to *n*-hexane, (−13.5 ± 0.2 kcal/mol), can be explained in terms of the larger conformational freedom of the *n*-hexane molecule and slightly higher polarizability α of *n*-hexane ($\alpha = 11.9 \times 10^{-24}$ cm^3 taken from Ref. [54] and 12.7×10^{-24} cm^3 from our DFT calculation, refer to Table S1 for calculated polarizabilities of all studied molecules) with respect to cyclohexane ($\alpha = 11.0 \times 10^{-24}$ cm^3 from Ref. [54] and 10.9×10^{-24} cm^3 from DFT calculation, Table S1). The higher conformational freedom enabled better fitting of *n*-hexane to the graphene surface. The higher polarizability leads to stronger London dispersive forces, which drive the adsorption of non-polar organic molecules to graphene [8]. The difference between cyclohexane and *n*-hexane was confirmed by our DFT calculation, which yielded adsorption enthalpies of −11.5 kcal/mol and −13.6 kcal/mol, respectively. These results corroborated the experimental data, thereby verifying that the difference in adsorption enthalpy stems from the difference in structure and character of cyclohexane and *n*-hexane.

The adsorption enthalpy of 1,4-dioxane, (−10.8 ± 0.1 kcal/mol), is slightly higher than the adsorption enthalpy of cyclohexane,

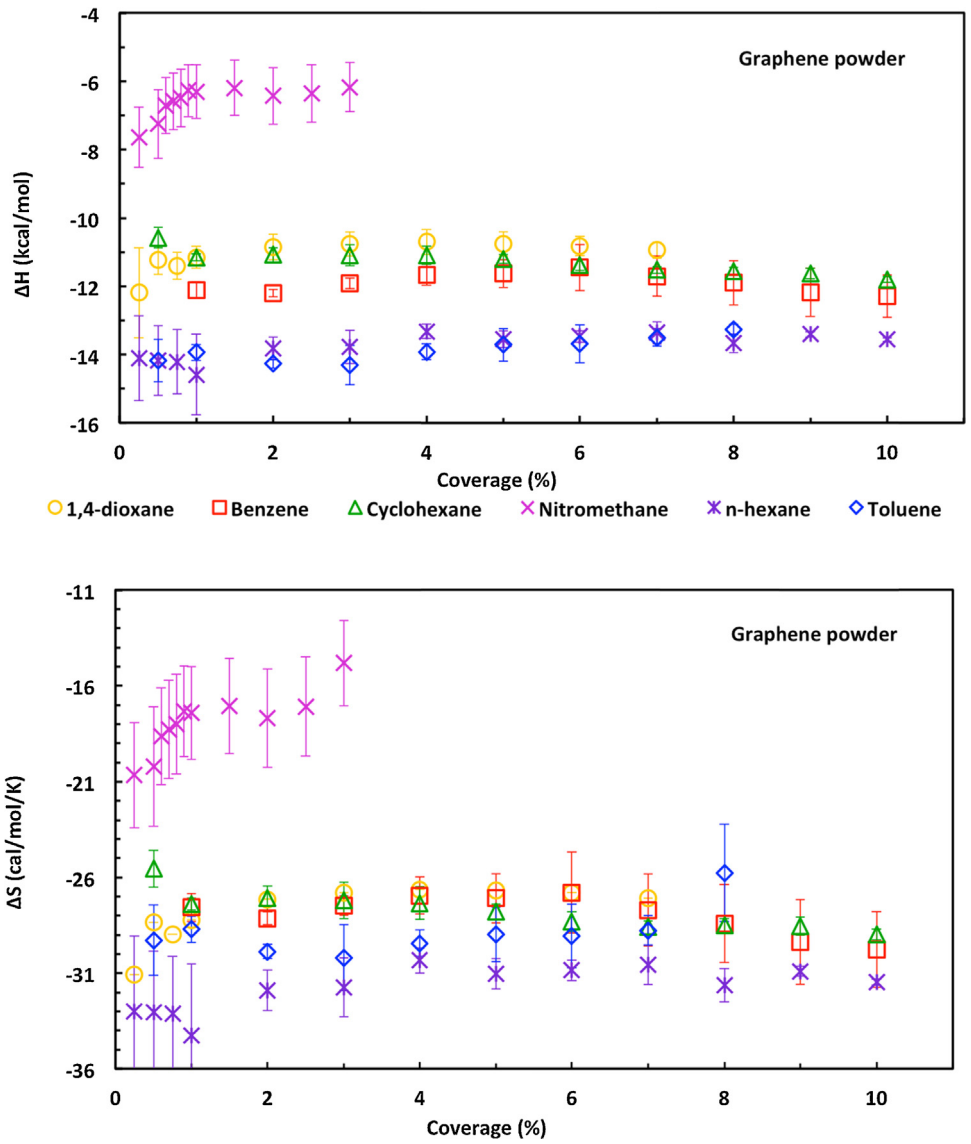

Fig. 3. IGC-determined isosteric adsorption enthalpy and entropy of molecular probes to graphene powder for coverages ranging from 0.25% to 10% of a monolayer (for some molecules, we extended the plot to 20% coverage, see Fig. S2 of the Supporting Information).

indicating that the enthalpy changes only modestly with oxygen substitution of two methylene groups. The adsorption enthalpy of aromatic benzene, (-11.9 ± 0.3 kcal/mol), is by a fraction lower than that of its saturated counterpart cyclohexane. However, according to experimental measurements, benzene is less polarizable than cyclohexane [54], so the higher affinity of benzene to graphene cannot be attributed solely to the London dispersive forces. Since benzene bears permanent quadrupole moment [55] (while quadrupole moment of cyclohexane is negligible) and that electrostatics contributes by ~30% to binding to graphene [8], the higher affinity of benzene can be explained by the higher contribution of electrostatics. This documents that the adsorption enthalpy to graphene is driven by a subtle interplay among individual contributions to the noncovalent interactions. Our DFT calculation yields the adsorption enthalpy of -11.7 kcal/mol for benzene, lower than that of cyclohexane (-11.5 kcal/mol) in line with the IGC result. Nevertheless, even the calculation cannot ultimately distinguish, which of the contributions to the adsorption promotes adsorption of benzene over cyclohexane. Toluene contains one more methyl group than benzene and, accordingly, has higher polarizability ($\alpha = 12.3 \times 10^{-24}$ cm^3 taken from Ref. [54] and 12.6×10^{-24} cm^3 from our DFT calculations, Table S1) and lower adsorption enthalpy (-13.8 ± 0.4 kcal/mol). The calculated adsorption enthalpy of toluene of -14.5 kcal/mol corroborates its strong adsorption on graphene.

3.3. *Adsorption enthalpies to fluorographene*

In the case of graphite fluoride, we obtained relatively stable adsorption enthalpies even for the small probe, nitromethane (Fig. 4). This is indicative of either a low fraction of high-energy sites or a similarity between the binding energy to steps/cavities and the binding energy to the fluorographene surface. In other words, these structural features, i.e., steps and/or cavities, do not create high-energy sites on this material for the molecules we used. Graphite fluorite consists of flaky lamellar crystals with exposed terraces composed of fluorographene layers (cf. Figs. 1 and 2). It is reasonable to assume that the adsorption process occurs predominantly on these exposed terraces, i.e., on the fluorographene. The observed adsorption enthalpies to fluorographene can therefore be attributed to adsorption to graphite fluoride terraces Fig. 5 shows optimized orientations of benzene

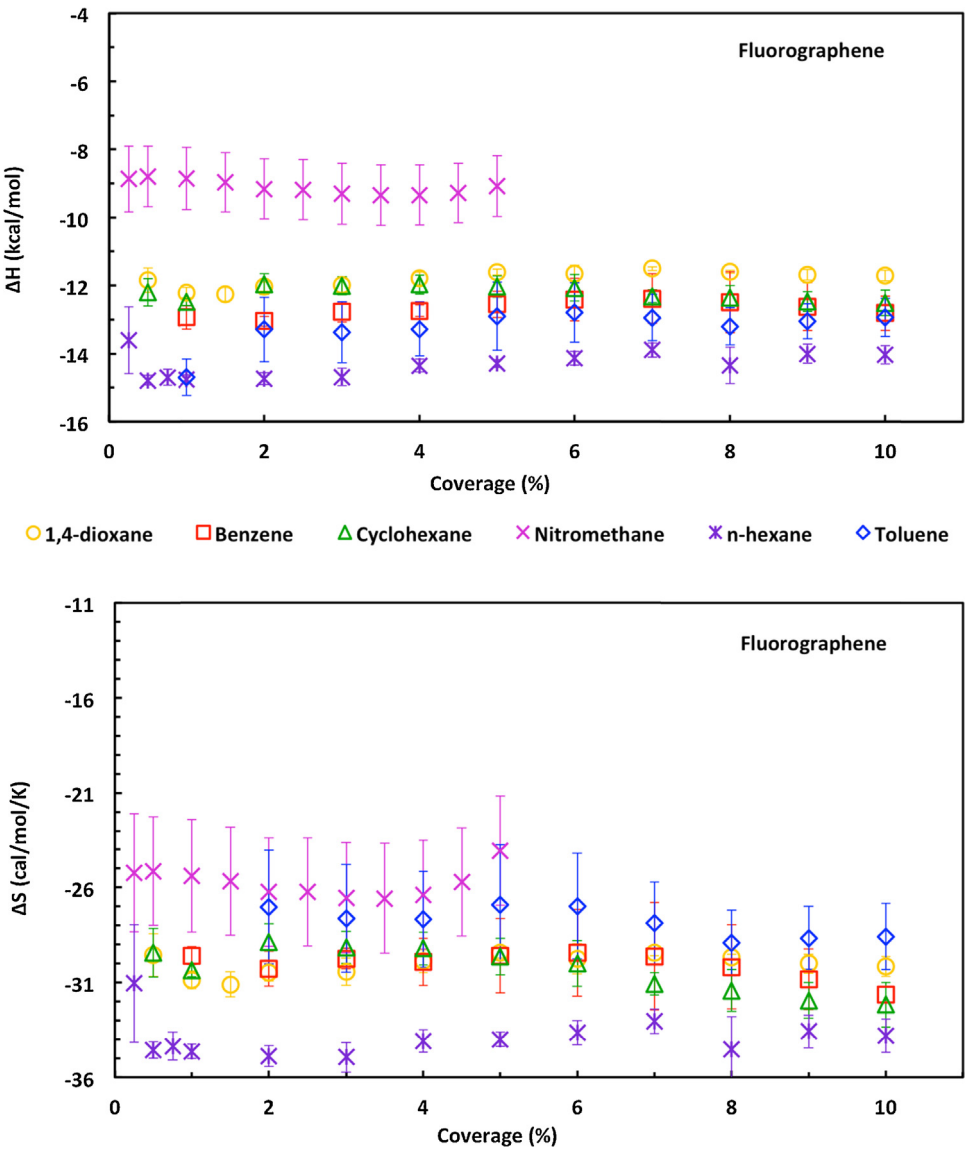

Fig. 4. IGC-determined isosteric adsorption enthalpies and entropies of selected molecular probes to graphite fluoride powder for coverages ranging from 0.25% to 10% of a monolayer (for some molecules we extended the plot up to 20% coverage, see Fig. S3 of the Supporting Information).

on both graphene and fluorographene surfaces. The calculated adsorption enthalpy of cyclohexane, *n*-hexane and benzene to single-layer fluorographene was −11.0 kcal/mol, −12.5 kcal/mol, and −10.2 kcal/mol, respectively. The calculation identifies toluene as the most strongly adsorbed molecule on fluorographene (−13.2 kcal/mol). Interestingly, the calculation ascribes stronger binding onto fluorographene to cyclohexane than to benzene, in contrast to the binding on graphene (see above). The axial C–H bonds of cyclohexane fit well into C–F pockets on fluorographene, which diminishes the advantage of flat geometry of benzene.

Comparing adsorption on fluorographene and graphene as seen in IGC experiment, the same relative trends were observed. For example, *n*-hexane had lower adsorption enthalpy, (−14.3 ± 0.3 kcal/mol), than cyclohexane (−12.2 ± 0.2 kcal/mol) and 1,4-dioxane (−11.7 ± 0.2 kcal/mol). Similarly, toluene had lower adsorption enthalpy, (−13.1 ± 0.2 kcal/mol), than benzene (−12.7 ± 0.2 kcal/mol). The only exception was that toluene had the lowest adsorption enthalpy to graphene, while *n*-hexane was the most strongly bound molecule to the fluorographene. The differences in adsorption enthalpy were governed by differences in molecular polarizabilities, i.e., London dispersive forces. More importantly, the adsorption enthalpies to fluorographene were slightly lower than those to graphene by ~9% (except for the adsorption enthalpy of toluene). That is a somewhat surprising result, because flurographene has lower surface energy than graphene [24]. It should be, however, noted that the adsorption enthalpies are controlled by a delicate balance among attractive and repulsive forces, which implies that there is not any direct relation between the cohesive (or surface) energy and the adsorption enthalpy of an adsorbate. Furthermore, the results indicate that the π electrons of graphene do not provide any significant contribution to the binding of small neutral molecules. It should be mentioned that similar conclusion was proposed by Grimme, who studied the interaction between stacked aromatic units and saturated (hydrogenated) rings of the same size. He found that the effect of the π system is rather subtle, and interactions between aromatic and saturated fragments of the same size are similarly strong [56].

3.4. Adsorption entropies to graphene and fluorographene

Using Langmuir adsorption model, we also determined the adsorption entropies from IGC experiments by fitting the primary

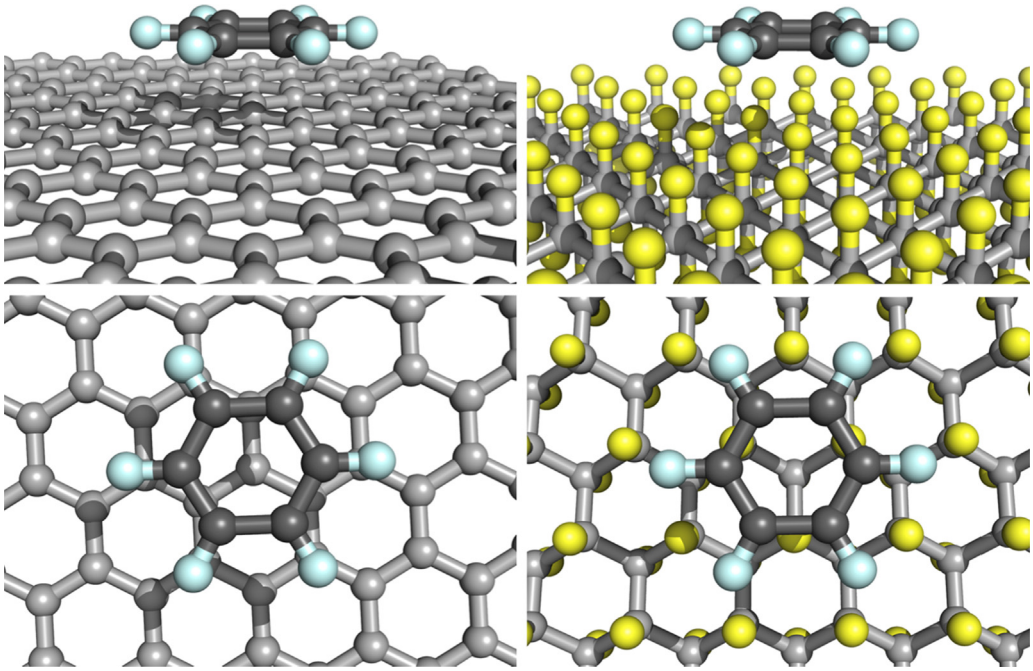

Fig. 5. Structures of benzene on graphene (left) and fluorographene (right) surfaces show that benzene ring is parallel to and lies 315 and 312 pm above the graphene and fluorographene surfaces, respectively. Carbon atoms are in gray, fluorine atoms in yellow and hydrogens in pale cyan.

data (cf. Methods). To best of our knowledge, IGC has not been used to determine and compare the adsorption entropies of several adsorbates yet. Measured adsorption entropies of ~−30 cal/mol K were obtained, although a higher value (−16.8 ± 1.1 cal/mol K) resulted for nitromethane on graphene. The lower adsorption entropy, at low coverage, of nitromethane on graphene confirms that the entropy loss is highest at the high-energy sites, where strong bonding restricts molecular motion [57]. The adsorption entropies exhibited similar trends to the adsorption enthalpies (the mean coefficient of determinations, r^2, of isosteric adsorption enthalpies vs. entropies were 0.78 and 0.69 for graphene and fluorographene, respectively). Furthermore, the entropies on fluorographene were only slightly lower (by ~10%) than those on graphene (with one exception, toluene). The adsorption entropies follow the adsorption enthalpies, which might indicate that stronger the binding the higher the configurational space restriction. It should be noted that the number of determined entropies is somewhat limited to make general conclusions and should be subject of further research. It was suggested that the surface entropies follow the adsorbates gas phase entropies [58]. In our case, the entropy loss corresponded to ~40% of the ideal gas phase entropy of the organic molecules S_g, which follows the trend observed for metal oxide surfaces [58].

4. Conclusion

Using the IGC technique, we determined the isosteric adsorption enthalpies and entropies of six volatile organic compounds to graphene and fluorographene as a function of the surface coverage. The results obtained for the smallest molecule used, i.e., nitromethane, indicated that graphene contained high-energy sites. On the other hand, the adsorption enthalpies and entropies of bulkier molecules were relatively coverage-independent. Nitromethane had the highest adsorption enthalpies and entropies on both graphene and fluorographene. The strongest binding was observed on graphene for toluene, and on fluorographene for *n*-hexane. The adsorption enthalpies were driven mainly by polarizabilities of individual molecules, i.e., London dispersive forces. The molecules on average exhibited lower adsorption enthalpies to fluorographene than to graphene and this finding was corroborated by DFT calculations. The adsorption entropies to graphene and fluorographene followed the adsorption enthalpies and corresponded to ~40% of negative gas phase entropies. The adsorption-induced entropy loss was highest at high-energy sites. In general, the used probes have rather strong affinities to both materials corresponding to ~10–15% of a common covalent bond and the affinities increased with molecular size and polarizability. The high affinities explain the fact that airborne contaminants readily adsorb on the surfaces and in turn modify surface properties as observed experimentally [9,10]. In addition, the organic probes have on average higher affinity to fluorographene than to graphene, which implies an effective usage of fluorographene in applications, where a direct contact with the molecular probe is required, e.g., electrochemical sensing [27–29]. On the other hand, the high-affinity warns that measured surface properties of fluorographene might be affected by adsorbed airborne contaminants.

Acknowledgements

Financial support from the Ministry of Education, Youth and Sports of the Czech Republic, via projects LO1305 and CZ.1.05/2.1.00/19.0377, is gratefully acknowledged. M.O. is funded by the European Union's Horizon 2020 research and innovation programme under ERC-CoG-2015 (grant No. 683024).

Appendix A. Supplementary data

Supplementary data associated with this article can be found, in the online version, at doi:10.1016/j.apmt.2016.09.016.

References

[1] K.S. Novoselov, et al., Electric field effect in atomically thin carbon films, Science 306 (5696) (2004) 666–669.
[2] K.S. Novoselov, et al., A roadmap for graphene, Nature 490 (7419) (2012) 192–200.

[3] V. Georgakilas, et al., Functionalization of graphene: covalent and non-covalent approaches, derivatives and applications, Chem. Rev. 112 (11) (2012) 6156–6214.
[4] F. Schwierz, Graphene transistors, Nat. Nanotechnol. 5 (7) (2010) 487–496.
[5] F. Schedin, et al., Detection of individual gas molecules adsorbed on graphene, Nat. Mater. 6 (9) (2007) 652–655.
[6] G.S. Kulkarni, et al., Electrical probing and tuning of molecular physisorption on graphene, Nano Lett. 16 (1) (2016) 695–700.
[7] J.D. Fowler, et al., Practical chemical sensors from chemically derived graphene, ACS Nano 3 (2) (2009) 301–306.
[8] P. Lazar, et al., Adsorption of small organic molecules on graphene, J. Am. Chem. Soc. 135 (16) (2013) 6372–6377.
[9] Z.T. Li, et al., Effect of airborne contaminants on the wettability of supported graphene and graphite, Nat. Mater. 12 (10) (2013) 925–931.
[10] D. Martinez-Martin, et al., Atmospheric contaminants on graphitic surfaces, Carbon 61 (2013) 33–39.
[11] G.K. Ramesha, et al., Graphene and graphene oxide as effective adsorbents toward anionic and cationic dyes, J. Colloid Interface Sci. 361 (1) (2011) 270–277.
[12] J.M.D. Tascon, Overview of carbon materials in relation to adsorption, Adsorp. Carbons (2008) 15–49.
[13] J. Xu, L. Wang, Y.F. Zhu, Decontamination of bisphenol A from aqueous solution by graphene adsorption, Langmuir 28 (22) (2012) 8418–8425.
[14] T.H. Liu, et al., Adsorption of methylene blue from aqueous solution by graphene, Colloids Surf. B Biointerfaces 90 (2012) 197–203.
[15] D.W. Johnson, B.P. Dobson, K.S. Coleman, A manufacturing perspective on graphene dispersions, Curr. Opin. Colloid Interface Sci. 20 (5–6) (2015) 367–382.
[16] A. Mohamed, et al., Graphene-philic surfactants for nanocomposites in latex technology, Adv. Colloid Interface Sci 230 (2016) 54–69.
[17] J.T. Robinson, et al., Properties of fluorinated graphene films, Nano Lett. 10 (8) (2010) 3001–3005.
[18] R.R. Nair, et al., Fluorographene: a two-dimensional counterpart of teflon, Small 6 (24) (2010) 2877–2884.
[19] R. Zboril, et al., Graphene fluoride: a stable stoichiometric graphene derivative and its chemical conversion to graphene, Small 6 (24) (2010) 2885–2891.
[20] M. Dubecky, et al., Reactivity of fluorographene: a facile way toward graphene derivatives, J. Phys. Chem. Lett. 6 (8) (2015) 1430–1434.
[21] V. Urbanova, et al., Thiofluorographene-hydrophilic graphene derivative with semiconducting and genosensing properties, Adv. Mater. 27 (14) (2015) 2305–2310.
[22] K.E. Whitener, et al., Graphene as electrophile: reactions of graphene fluoride, J. Phys. Chem. C 119 (19) (2015) 10507–10512.
[23] P. Lazar, et al., Dichlorocarbene-functionalized fluorographene: synthesis and reaction mechanism, Small 11 (31) (2015) 3790–3796.
[24] P. Lazar, et al., The surface and structural properties of graphite fluoride, Carbon 94 (2015) 804–809.
[25] R.L. Fusaro, H.E. Sliney, Graphite fluoride $(Cfx)_N$ – new solid lubricant, ASLE Trans. 13 (1) (1970) 56.
[26] S. Kwon, et al., Enhanced nanoscale friction on fluorinated graphene, Nano Lett. 12 (12) (2012) 6043–6048.
[27] X.Y. Chia, et al., Fluorographites (CFx)(n) exhibit improved heterogeneous electron-transfer rates with increasing level of fluorination: towards the sensing of biomolecules, Chem. Eur. J. 20 (22) (2014) 6665–6671.
[28] V. Urbanova, et al., Fluorinated graphenes as advanced biosensors – effect of fluorine coverage on electron transfer properties and adsorption of biomolecules, Nanoscale 8 (24) (2016) 12134–12142.
[29] K.K. Tadi, S. Pal, T.N. Narayanan, Fluorographene based ultrasensitive ammonia sensor, Sci. Rep. 6 (2016).
[30] T.V. Vineesh, et al., Synergistic effects of dopants on the spin density of catalytic active centres of N-doped fluorinated graphene for oxygen reduction reaction, Appl. Mater. Today 1 (2) (2015) 74–79.
[31] H.L. Poh, et al., Fluorographenes via thermal exfoliation of graphite oxide in SF_6, SF_4, MoF_6 atmospheres, J. Mater. Chem. C 2 (26) (2014) 5198–5207.
[32] V. Mazanek, et al., Tuning of fluorine content in graphene: towards large-scale production of stoichiometric fluorographene, Nanoscale 7 (32) (2015) 13646–13655.
[33] W.Z. Teo, et al., Cytotoxicity of fluorographene, RSC Adv. 5 (129) (2015) 107158–107165.
[34] W.Z. Teo, et al., Fluorinated nanocarbons cytotoxicity, Chem. Eur. J. 21 (37) (2015) 13020–13026.
[35] L. Spanu, S. Sorella, G. Galli, Nature and strength of interlayer binding in graphite, Phys. Rev. Lett. 103 (19) (2009).
[36] A.K. Geim, K.S. Novoselov, The rise of graphene, Nat. Mater. 6 (3) (2007) 183–191.
[37] E.M. Perez, N. Martin, pi–pi interactions in carbon nanostructures, Chem. Soc. Rev. 44 (18) (2015) 6425–6433.
[38] V. Georgakilas, et al., Noncovalent functionalization of graphene and graphene oxide for energy materials, biosensing, catalytic, and biomedical applications, Chem. Rev. 116 (9) (2016) 5464–5519.
[39] Y. Sato, et al., On the so-called "semi-ionic" C–F bond character in fluorine-GIC, Carbon 42 (15) (2004) 3243–3249.
[40] F. Karlicky, M. Otyepka, Band gaps and optical spectra of chlorographene, fluorographene and graphane from G(0)W(0), GW(0) and GW calculations on top of PBE and HSE06 orbitals, J. Chem. Theory Comput. 9 (9) (2013) 4155–4164.
[41] R. Ho, J.Y.Y. Heng, A review of inverse gas chromatography and its development as a tool to characterize anisotropic surface properties of pharmaceutical solids, Kona Powder Part. J. (30) (2013) 164–180.
[42] S. Mohammadi-Jam, K.E. Waters, Inverse gas chromatography applications: a review, Adv. Colloid Interface Sci. 212 (2014) 21–44.
[43] H. Balard, et al., Study by inverse gas chromatography of the surface properties of milled graphites, J. Chromatogr. A 1198 (2008) 173–180.
[44] H. Balard, Estimation of the surface energetic heterogeneity of a solid by inverse gas chromatography, Langmuir 13 (5) (1997) 1260–1269.
[45] E. Papirer, et al., Comparison of the surface properties of graphite, carbon black and fullerene samples, measured by inverse gas chromatography, Carbon 37 (8) (1999) 1265–1274.
[46] F. Karlicky, et al., Interplay between ethanol adsorption to high-energy sites clustering on graphene graphite alters the measured isosteric adsorption enthalpies, J. Phys. Chem. C 119 (35) (2015) 20535–20543.
[47] M. Pykal, et al., Modelling of graphene functionalization, Phys. Chem. Chem. Phys. 18 (9) (2016) 6351–6372.
[48] P. Lazar, et al., The nature of high surface energy sites in graphene and graphite, Carbon 73 (2014) 448–453.
[49] P.E. Blochl, Projector augmented-wave method, Phys. Rev. B 50 (24) (1994) 17953–17979.
[50] G. Kresse, D. Joubert, From ultrasoft pseudopotentials to the projector augmented-wave method, Phys. Rev. B 59 (3) (1999) 1758–1775.
[51] J. Klimes, D.R. Bowler, A. Michaelides, Van der Waals density functionals applied to solids, Phys. Rev. B 83 (19) (2011).
[52] H. Ulbricht, et al., Thermal desorption of gases and solvents from graphite and carbon nanotube surfaces, Carbon 44 (14) (2006) 2931–2942.
[53] R. Zacharia, H. Ulbricht, T. Hertel, Interlayer cohesive energy of graphite from thermal desorption of polyaromatic hydrocarbons, Phys. Rev. B 69 (15) (2004).
[54] W.M. Haynes, CRC Handbook of Chemistry and Physics, 93rd ed., CRC Press, 2016.
[55] J. Vrbancich, G.L.D. Ritchie, Quadrupole-moments of benzene, hexafluorobenzene and other non-dipolar aromatic-molecules, J. Chem. Soc. Farad. Trans. II 76 (1980) 648–659.
[56] S. Grimme, Do special noncovalent π–π stacking interactions really exist? Angew. Chem. Int. Ed. 47 (18) (2008) 3430–3434.
[57] C.T. Campbell, J.R.V. Sellers, The entropies of adsorbed molecules, J. Am. Chem. Soc. 134 (43) (2012) 8109–18115.
[58] C.T. Campbell, J.R.V. Sellers, Enthalpies and entropies of adsorption on well-defined oxide surfaces: experimental measurements, Chem. Rev. 113 (6) (2013) 4106–4135.